Progress In Electromagnetics Research C, Vol. 123, 181–196, 2022

Statistical Analysis of Diffraction Loss in Outdoor Urban Microcells for 5G/6G Millimeter Wave Communications

Abdelbasset Bedda Zekri and Riadh Ajgou*

Abstract—Millimeter-wave (mmWave) frequencies are considered as candidate bands for 5G/6G mobile networks. Diffraction models are significant for predicting non-line-of-sight (NLOS) wireless channels while it is shown that the line of sight (LOS) path is usually blocked by buildings in urban area environments. A lot of investigations on the diffraction loss have been performed, and most of them just considered one obscuring object and a short propagation distance. In this paper, we conduct a statistical analysis of the diffraction loss in the outdoor NLOS in Urban Micro Cell, considering a transmitter (TX) and a receiver (RX) which are located at an aggregation point on the roof of a building. We have focused on analyzing the diffraction loss suffered by mmWave signals when they hit one or two obscuring points located over rooftop of the buildings. The objects have different heights located at various distances between TX and RX. We have considered the bands: 28 GHz, 38 GHz, 60 GHz, 73 GHz, and 100 GHz. The analysis is based on the diffraction model named Knife Edge Diffraction (KED). We have strictly followed the ITU Recommendations ITU-R P.526-15 (10/2019). In this work, we use two schemes that characterize the KED model, namely Single KED (SKED) and Double Isolated KED (DIKED). Different scenarios are performed by varying different parameters of the channel between TX and RX. The results show that the diffraction loss is inversely proportional to the distance between the obscuring object and the transmitter, the wavelength, and the distance between the TX and RX.

1. INTRODUCTION

The wireless deployment of 5G has already started in certain countries. However, some technical problems that need to be updated and further technological improvements are needed. On the other hand, we have to take into consideration the use of 6G, because of the technological evolution, the society and the vision of the world in the 2030s as soon as 6G will be proposed. Obviously, a wider diffusion will be necessary as a type of promoting progress in the 2030s. Furthermore, additional advanced services will require the combination of various use cases and new use cases as well as increasing the signal processing rate and the development of various devices that require ultra-high speed of numerous gigabits per second for data communications via bandwidth of gigahertz, which is remarkably wider than that obtained previously in 5G.

We note that it is difficult to obtain a wide range of frequencies to develop 5G/6G wireless networks because of the density of frequency used by many technological applications. Using millimeter waves (mmWave) may provide broadband requirements for future 5G/6G networks.

The mmWave frequency bands have been considered between 30 and 300 GHz. To meet the high bit rate requirements of mobile networks (5G/6G), mmWave frequencies are likely to be used. Because mmWave is exposed to losses during propagation in harsh environments such as loss of diffraction, it has not been used before in mobile networks. In new 5G radios, frequency ranges up to 52.6 GHz are adopted, and other bands around 100 GHz are being considered for the next version (6G) [1], where the focus is on the lower bands at 60 GHz or at most 90 GHz. In fact, the use of frequencies below

Received 20 May 2022, Accepted 16 August 2022, Scheduled 30 August 2022
* Corresponding author: Riadh Ajgou (riadh-ajgou@univ-eloued.dz).
The authors are with the LEVRES Laboratory, Department of Electrical Engineering, University of El Oued, El-Oued 39000, Algeria.

100 GHz by recent technologies was very rare until recently. The United States Federal Communications Commission (FCC) recommends that higher frequencies, such as 95 GHz at 3 THz, be well thought-out for 6G [1, 2]. In order to achieve extremely high data rates exceeding several 1 Gbps, researchers are exploring these high frequency bands, from the top of the millimeter wave band to the terahertz wave range. Otherwise, it is assumed that radio waves up to about 300 GHz are taken into account in the 6G assessment range.

For ideal 6G/5G development, channel parameters must be studied in different environments to determine mobile network engineering, type of antennas, design, deployments, etc. In addition, electromagnetic problems such as scattering and diffraction problems have been widely studied. More details about propagation characteristics and problems of mmWaves were provided in [3].

In [4], the authors proposed a node-based discontinuous Galerkin (DG) pseudospectral time domain (PSTD) algorithm, with adaptive nonconformal unstructured meshes, for 3-D large-scale Maxwell's equations, in which an adaptive application of 5G electromagnetic signal propagation demonstrates the effectiveness and aptitude of the developed high-order solver. This new DG-PSTD algorithm has been mathematically confirmed to be long-time stable for curvilinear mappings by the application of math community, but it is still ambiguous why the standard DG-PSTD formulation works good for mechanical waves, but not for electromagnetics. In computational electromagnetics, face/edge elements are the most common ways to discretize the electric field intensity E (or magnetic field intensity H) in the Finite Element Method (FEMs). However, it is nontrivial to extend them to higher orders [5]. In [5], the authors proposed a stabilized nodal discontinuous Galerkin pseudospectral time-domain (DG-PSTD) algorithm for entirely anisotropic electromagnetic waves.

With the fast growth of wireless mobile communication (5G/6G), the dimension of a cell turns out to be smaller, thus in this work we have considered Urban Microcells in NLOS propagation with the existence of buildings. The outdoor environment determined as one of the significant application scenarios in mobiles communications [3]. In an urban environment, obstructions from the presence of buildings and also human blockage strongly affect radio propagation [6, 7]. The presence of buildings in these environments causes defy to model path loss and estimating the influence on the signal reception in the NLOS propagation due to several fundamental propagation factors (i.e., reflection, diffraction, and scattering). Investigations on mmWave propagation characteristics are necessary for designing and assessing 5G/6G systems and start on 5G/6G services by analyzing the mmWave loss factors due to diffraction during propagation on the roof of buildings. For example, obstruction due to clutter frequently takes place in mobile networks environments; for that reason, the diffraction loss is a serious propagation characteristic of 5G/6G systems. Diffraction loss in urban microcell leads to the loss of transmission power, hence the transmitted information quality and the quality of service (QoS) of networks and application.

Diffraction is defined as a phenomenon that occurs when an electromagnetic (EM) wave hits an obstacle or a slit. Moreover, it is considered as the bending of waves around the obstacle angles or through an opening in the area of the geometric obstacle/aperture shadow. Because of the use of mmWave that is more affected by environment, the diffraction loss over a building rooftop is a decisive issue when signal levels are predicted. Diffracted wave in urban microcell is able to arrive at the receiver even if the transmitter and receiver are not in line of sight (LOS) and can lead to strengthening and weakening of the received signal irregularly. As a secondary wavelet is produced because of diffraction, the diffracted wave signal strength will be less than the reflected signal. The authors in [8] explain the propagation characteristics effect on free space loss due to the movement of surrounding objects or the location of receivers in the open area of the mmWave bands (28 GHz, 38 GHz) for 5G system.

Otherwise, the diffraction losses determination with a minimum suitable error is extremely difficult for realistic propagation environments, thus system design needs a set of statistics which expresses the likely performance of a propagation path. Propagation models are employed to offer the essential statistics [9]. The line-of-sight (LOS) between the transmitter and receiver is easily blocked by an edifice in mobile network environments, mainly in urban areas where diffraction loss is very high in predicting wireless propagation behaviors in different non-line-of-sight (NLOS) environments [10, 11]. The propagation loss model for roof propagation is assessed in [10]; otherwise considering diffraction models, the authors in [12] proposed the propagation loss model after street corners. Based on a ray-tracing simulation, in [11] the authors proposed a mmWave channel model as well as rapid fading and

path loss.

Theoretical models have been suggested in [13–15] to predict propagation of EM waves in the scenario of NLOS outdoor/indoor urban area.

For Geometric Optics (GO) in terms of direct, reflected, and refracted waves, the Fermat standard presents a theory of propagation. On the other hand, the GO is limited to predict the propagation losses to the NLOS points where the reflected waves and refracted do not reach. To develop the GO, the geometric theory of diffraction (GTD) was suggested in [16] along a new category of waves diffracted from the border of obscuring objects. Using Huygens principle, the diffraction could be demonstrated where each point of the EM waves turns out to be a new source of a spherical wave which means that the EM waves can arrive at any point in the NLOS area by diffraction. GTD models feature a new source of diffracted waves at every corner of obstruction. While GTD models are able to expect propagation losses across all NLOS areas, they have a problem of singular transitions at shaded borders. To defeat this, the uniform geometrical theory of diffraction (UTD) has been projected with an analysis based on [15].

These types of theories of GTD and UTD that are able to effectively provide the prediction of the loss, however, do not involve the consideration of circular wave sources in all areas, but include source considerations only at the edge of the obstruction. This dynamic single-source diffracted wave assumption may be inaccurate in the case of extended distances. Therefore, to improve and validate long-distance theoretical models, diffraction measurement estimates in a variety of areas are essential.

Toward expanding and confirming diffraction models, numerous studies on diffraction losses have been carried out [17–25].

The measurements of diffraction loss over distances of approximately several kilometers in length at the top of a mountain at 0.1 to 10 GHz are provided in [17], but angles of the diffraction do not exceed 3 degrees. The 28 GHz diffraction loss model based on rooftop propagation measurements from a distance range up to about 150 m and the diffraction angle range up to about 50 degrees is provided in [18], but it is limited by measurements under one roof of the building.

The authors in [19] performed diffraction loss measurements at 28 GHz, 32.4 GHz, and 38 GHz where a millimeter wave is propagated on the roof of a building by diffraction. The results of measurements and theoretical models are also compared in [19], such as the Knife Edge Diffraction (KED) model and GTD model. The measurement results showed high losses compared to the KED model, in particular with high Fresnel-Kirchhoff diffraction parameters. In high frequency environments, long distances, and high diffraction angles, the high Fresnel-Kirchoff diffraction parameters are realized. Diffraction measurements in the region of an angle of a building have been presented in [20–23]. The diffraction losses in [20–22] were carried out at frequencies from 10 GHz to 60 GHz, but limited by the propagation distances less than 10 m. The diffraction losses in [23] were performed at a low frequency of 1.823 GHz.

A lot of investigations on the diffraction loss have been performed; however, most of these investigations just considered one obscuring object and a short propagation distance, and this paper investigates the diffraction loss for a selected mmWave bands in Outdoor Urban Microcells. In this context, we have investigated the diffraction path loss in an outdoor urban micro-cell based on the propagation on the roof of a building, where we focused on the diffraction loss experienced by millimeter wave signals when they hit one or two obscuring points located on the roof of a building having different heights located at diverse distances between a transmitter (TX) and a receiver (RX), considering 28 GHz, 38 GHz, 60 GHz, 73 GHz, and 100 GHz bands. The simulation was based on KED model. In KED model we can summarize two diffraction models known as the single knife diffraction model (SKED) and Double Isolated Single Knife Edge Diffraction (DISKED) where we focus on ITU Recommendation ITU-R P.526-15 (10/2019).

This work is arranged as follows. Section 2 introduces diffraction models with more details. Section 3 presents simulation results to analyze the diffraction loss on selected mmWave bands. Finally, Section 4 provides concluding remarks.

2. DIFFRACTION LOSS MODELS

Most research on propagation loss uses Knife Edge diffraction (KED) and Uniform Geometric Diffraction Theory (UTD) models to simulate the loss of diffraction by considering the corners and roofs of edge

buildings.

KED relies on perfect conductivity and provides an approximation formula for the edge diffraction. The diffracted electric field with reference to the electric field received from an isotropic radiator in the absence of the obstructing edge can be calculated using the Fresnel integral KED (Equation (3)), and reasonable accuracy is reported below 6 GHz in [26] and at 60 GHz in [27]. In addition, It has been demonstrated experimentally that KED is sufficient to model human blockage at mmWave frequencies [26]. In addition, in [18] diffraction losses were measured when millimeter-waves propagated over a building rooftop. The height of the building was 14 m, and the carrier frequency was 28 GHz. The transmitter (TX) was located on the ground and the receiver (RX) located on the rooftop where the efficiency of KED model was confirmed.

The main objective of the analysis is to determine typical diffraction loss values and corresponding parametric values of the SKED model. This information is valuable input in the design of a NLOS small cell backhaul system.

In our work, we have considered the KED model.

2.1. KED (Knife Edge Diffraction) Model

As illustrated in Section 1, for the KED model, we have considered two schemes, namely SKED and DIKED.

2.1.1. Single Knife Edge Diffraction (SKED)

The model SKED shown in Fig. 1 treats two optimal conditions between the transmitter (TX) and receiver (RX) in which an extreme obstacle is placed. Diffraction loss can be quantified by a dimension less quantity known the Fresnel-Krichhoff diffraction parameter v using all geometric parameters as seen in this figure. The parameter v can be calculated according to ITU-R P.526-15 ITU-R P.526-15 (10/2019) using formulas (1), which depends on the availability of information [24].

$$\nu = h\sqrt{\frac{2}{\lambda}\left(\frac{1}{d_1}+\frac{1}{d_2}\right)} = \theta\sqrt{\frac{2}{\lambda\left(\frac{1}{d_1}+\frac{1}{d_2}\right)}} = \sqrt{\frac{2h\theta}{\lambda}} = \sqrt{\frac{2d}{\lambda}\cdot\alpha_1\alpha_2} \tag{1}$$

where:

h: distance between the top of the obstruction and the straight line joining the sides of the path. The value of h is in meter and has a negative sign if it is below the line of the path.

d_1, d_2: distances between the two ends of the path and the top of the obstruction in meter units.

d: the length of the path between the transmitter and the receiver, in the meter units.

θ: the angle of diffraction in radian unit with the same sign as h.

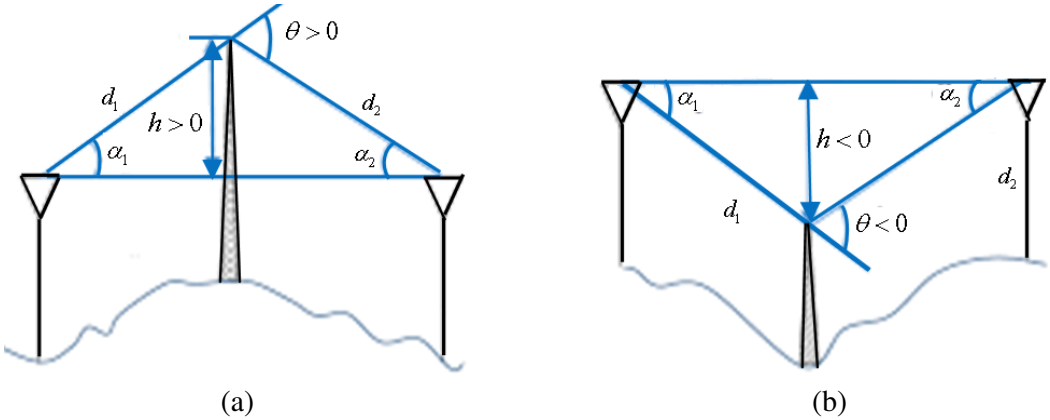

Figure 1. SKED obstacle: (a) h positive, (b) h negative [25].

α_1, α_2: angles between the lines that connect the top of the obstruction to the ends of the path and the horizon in radian.

After calculating the parameter v (Equation (1)), the signal level due to the SKED is obtained by integrating the contributions of the free portions of the wavefront. The diffraction loss $L(v)$ is obtained as:

$$L(\nu) = 20\log_{10}\left[0.5\sqrt{[1 - C(\nu) - S(\nu)]^2 + [C(\nu) - S(\nu)]^2}\right] \text{ [dB]} \tag{2}$$

where $C(v)$ and $S(v)$ are respectively the real and imaginary parts of the complex Fresnel integral $F(v)$ given by [24]:

$$F(\nu) = \frac{(1+j)}{2}\int_{\nu}^{\infty} \exp\left[\frac{-j\pi t^2}{2}\right] dt \tag{3}$$

Approximation given in Equation (4) can be used in a case where $v > -0.78$ [24].

$$L(\nu) = 6.9 + 20\log_{10}\left(\sqrt{(\nu - 0.1)^2 + 1} + v - 0.1\right) \text{ [dB]} \tag{4}$$

2.1.2. Double Isolated Single Knife Edge Diffraction (DISKED)

In the literature we found some works using DISKED as in [28] with a comparison of measured human-induced shadowing events and the prediction by a double knife-edge model at 60 GHz and 300 GHz. The distance between Tx and Rx was chosen as 2.7 m at 60 GHz and 1 m at 300 GHz (in our work we considered roof-building). The test heads have been mounted at a height at 1.10 m. For the prediction, the Double Knife-Edge Model has been applied, where a person is modelled by two knife edges at the front and the back of the body. The results show a good agreement at 60 GHz for the lit and shadow regions, whereas at 300 GHz the measured diffraction loss is lower than the predicted one in the deep shadow area, due to the limited dynamic range at 300 GHz. Results are in good agreement with the measurements.

A) Bullington Model

The Bullington model is shown in Fig. 2(a), and the intersection of two tangential lines from TX and RX antennas to their adjacent obstructions is supposed to be a similar knife-edge obstruction with height *hp*. This model is valid when the obstructions are near each other, and the obtained results are compatible to the experimental assessments [29]. The calculation of diffraction loss is computed using Equation (1). This model has the advantage of simplicity but obstacles under the paths of the horizon rays could be ignored. It is realized that Bullington model overestimates the double diffraction loss whilst the obstruction depth of the equivalent single edge is big in urban area [30].

B) Epstein and Peterson Models

The models of Epstein and Peterson are shown in Fig. 2(b), and the heights *hp*1 and *hp*2 should be obtained first, and then the sum of the corresponding knife-edge losses ought to be counted. When the distance between the obstacles is long, these models are accurate. While refraction or diffraction happens, amounts of loss that could be assigned to the obstruction depends on frequency. When numerous obstructions are found in the path, losses can be summed to define a residual level of radio energy at a far point. The Epstein-Peterson model offers a methodology for calculating such cumulative losses and giving residual signals [31].

C) Piquonard Model

As shown in Fig. 2(c), for this model method, first, one of the obstructions is omitted, and the knife-edge loss is determined on the basis of *hp*1 and d_1. Then the second knife-edge obstruction loss is determined on the basis of *hp*2 and d_2 for the path between the receiver and the first obstacle. Finally, the net loss is equal to the total of the losses from both knife-edge obstructions.

This model, with fewer restrictions, is more suitable than the previous methods [29]. In the range of 88–108 MHz, the authors in [32] studied two different versions of the Picquenard model. The first is the universal Piquonard model taking into account all terrain obstacles. The other takes the main diffraction

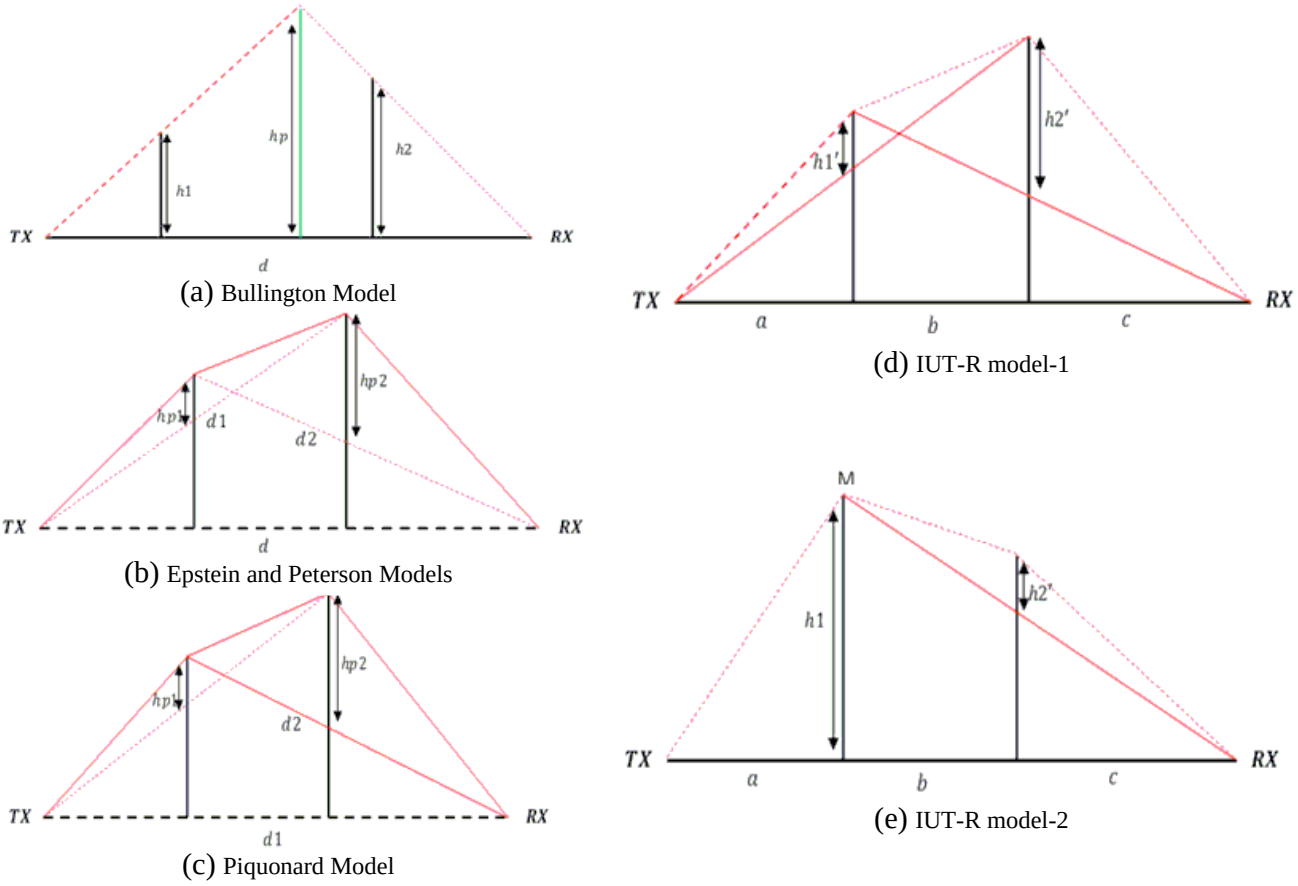

(a) Bullington Model

(b) Epstein and Peterson Models

(c) Piquonard Model

(d) IUT-R model-1

(e) IUT-R model-2

Figure 2. Double isolated single Knife-edge obstacle models.

term into account, with the addition of 0.67 multiplied by the next main diffraction term. Furthermore, in comparison with Epstein and Peterson models that provides perfect results just when diffractors are far apart; if not it is a poor predictor, where the models supposed that the totality excess loss for two diffractors can be considered as the sum of the individual losses calculated independently [33]. Besides, Piquonard model gets rid of the limits of models of Epstein and Peterson. The loss due to a double diffractor is achieved by first evaluating the loss because of the first diffractor whereas ignoring the second diffractor close to the receiver. The loss by the second diffractor is then designed on the supposition that the transmitter is situated on top of the first diffractor. The amount of these losses gives good estimate of definite diffraction loss.

D) ITU-R Model

The ITU models according to ITU-R P.526-15 (10/2019) are well illustrated in [24], and numerous models can study the effect of diffraction on the received field strength, as well as the usually utilized model KED. The model is appropriate to diverse nature of obstacle and to different path geometries [24]. This model consists of carrying out the theory of SKED to two obstacles successively, with the peak of the first one considering the source for diffraction over the second one.

In [34], the authors provide an extended version of the basic diffraction model in ITU-R P.526, applied in urban microcell environment, and illustrated the characteristics of path loss resulting from traffic sign blockage. Many frequency bands including mmWave frequency bands up to 40 GHz are investigated. Otherwise, in [3], more studies are provided about recommended parameters for diffraction loss models of ITU 526 in the case of wide range of mmWave bands in urban cell. In urban area, if the roof-top heights vary by a large amount further than the first Fresnel-zone radius, a chosen method is to use the highest buildings along the path in a knife-edge diffraction calculation, as described in

Recommendation ITU-R P.526 [3].

Figure 2(d) illustrates that the first diffraction way, identified by the ranges a and b and the altitude $h1'$, contributes a loss J_1 [dB]. The second diffraction way, identified by the ranges a and b and the altitude $h2'$, contributes a loss J_2 [dB]. The values J_1 and J_2 are obtained by the formula of Equation (2). A correction term J_c [dB] should be added to take into consideration the distance b between the edges. J_c can be evaluated by:

$$J_c = 10 \log \left[\frac{(a+b)(b+c)}{b(a+b+c)} \right] \tag{5}$$

which is applicable in case both J_1 and J_2 surpass about 15 dB. Finally, the overall diffraction loss of all obstructions is evaluated by the following expression:

$$J = J_1 + J_2 + J_c \tag{6}$$

In certain cases, the first model has a correct outcome, in which J_1 and J_2 have almost the same value.

As shown in Fig. 2(e), one of the obstructions is predominant and has more effects. In this model, the first diffraction way is related with parameters a, $(a+b)$, and $h1$, and the second diffraction way is related with parameters b, c, and $h2'$. The losses corresponding to them are obtained using Equation (2). Correction term T_c (dB) is evaluated by:

$$T_c = \left[12 - 20 \log_{10} \left(\frac{2}{1 - \frac{\alpha}{\pi}} \right) \right] \left(\frac{q}{p} \right)^{2p} \tag{7}$$

with:

$$p = \left[\frac{2}{\lambda} \frac{(a+b+c)}{(b+c)\,a} \right]^{1/2} h_1 \tag{8}$$

$$q = \left[\frac{2}{\lambda} \frac{(a+b+c)}{(a+b)\,c} \right]^{1/2} h_2 \tag{9}$$

$$\tan \alpha = \left[\frac{b(a+b+c)}{ac} \right]^{1/2} \tag{10}$$

h_1 and h_2 are the heights of edges corresponding to the direct way transmitter-receiver. The total diffraction loss is given by:

$$J = J_1 + J_2 - T_c \tag{11}$$

3. SIMULATION AND ANALYSIS OF RESULTS

In this part, we carry out numerical simulations to analyze the diffraction loss at 28 GHz, 38 GHz, 60 GHz, 73 GHz, and 100 GHz, considering one or two obscuring points located on the rooftop of building object. Obscuring points having different heights situated at different ranges in path connect a transmitter and a receiver. The analysis is performed by using SKED and DISKED models according to IUT recommendation.

3.1. Single Knife Edge Model

3.1.1. Effect of the Height h on the Diffraction Loss (L_{df})

Figure 3 illustrates the effect of the obstructing object height on the diffraction loss L_{df}. The values of d_1, d_2, and f were fixed at 40 m, 160 m, and 100 GHz, respectively. When the diffracting object is under the Line of sight way between TX and RX, which means h negative, the effect is low, but this effect increases as the top of diffracting object crosses the LOS way. At $h = 0$, L_{df} is about 6 dB. As h increases, the effect of the diffracting objects increases.

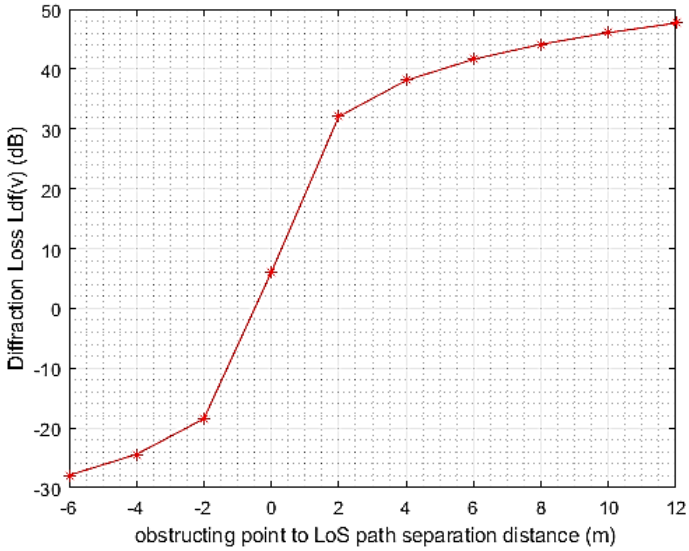

Figure 3. Effect of the height of diffracting object on diffraction loss.

3.1.2. Effect of Distance between TX and Diffracting Point on Diffraction Loss

In this simulation, we consider the effect of the distance between TX and obscuring point d_1 on diffraction loss employing various frequencies (28 GHz, 38 GHz, 60 GHz, 73 GHz, and 100 GHz), where h and d (distance TX/RX) are fixed at 12 m, 200 m, respectively. The distance d_1 is varied from 40 m to 160 m by step of 20 m, and the distance d_2 is given by:

$$d_2 = d - d_1 \text{ [m]} \tag{12}$$

A plot of L_{df} as a function of d_1 is shown in Fig. 4. We can see that the losses are larger as the obscuring object is near TX or RX antenna.

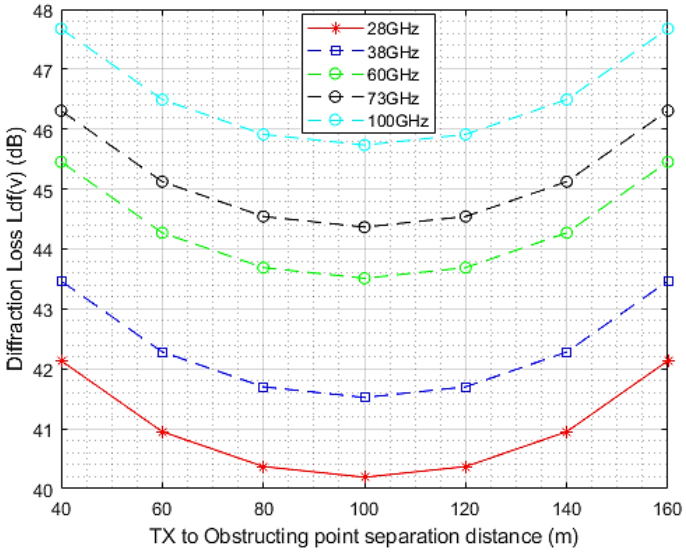

Figure 4. Effect of distance between TX and diffracting point on diffraction loss.

3.1.3. Effect of Wavelength on Diffraction Loss

Figure 5 shows the effect of wavelength on diffraction loss, where d_1 and h were set to the values 40 m and 12 m, respectively. The values of λ in this simulation are corresponding to the following frequencies (28 GHz, 38 GHz, 60 GHz, 73 GHz, and 100 GHz). This study is very significant because the distribution of spectrum bands for point-to-point links differs from country to country. We can see that the diffraction loss is inversely proportional to the wavelength.

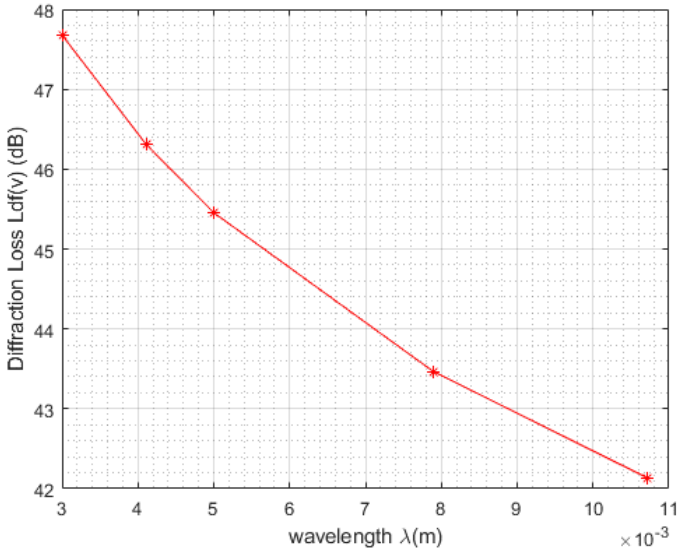

Figure 5. Effect of wavelength on diffraction loss.

3.1.4. Effect of TX/RX Separation Distance on Diffraction Loss

In this analysis, we suppose that TX/RX connection employed at frequency 100 GHz with different values of TX/RX distance (d) is used. h is set to 12 m. In each value of d (200 m, 400 m, 600 m, and 800 m), the distance d_1 was varied from 40 m to 180 m, 40 m to 360 m, 40 m to 560 m, and 40 m to 760 m,

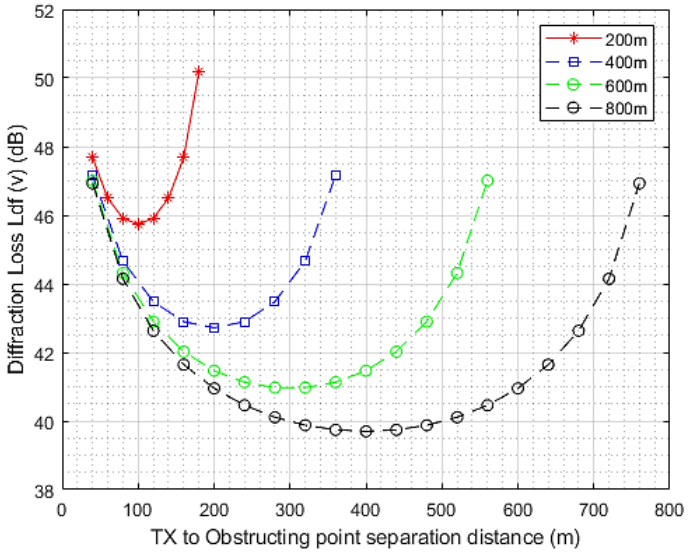

Figure 6. Effect of TX/RX separation distance on diffraction loss.

respectively. Fig. 6 shows the effect of TX/RX separation distance on diffraction loss. As shown in Fig. 6, all the plots have the same curvature for inter-site distances, and to optimize the coverage zone of the multipath mmWave connection, the site where the diffraction loss is very significant denotes the locations after which the mmWave link cannot search for diffracting points. The area that extends from the transmitter to receiver for a distance of 800 meters is considered as the most affected region by diffraction. This area is less affected as the length of the link increases.

3.2. Double Isolated Single Knife Edge Using ITU-R Model

3.2.1. Effect of the Height Ratio of Obstructing Object 2 Compare to 1 on Diffraction Loss

Figure 7 shows the effect the height ratio of the obstructing objects 1 and 2 on diffraction loss using ITU-R model. The values of a, b, c, and f were set to 40 m, 120 m, 40 m, and 100 GHz, respectively; h_1 is set to 120 m; and h_2 is varied from 2 m and 12 m. As the height ratio increases, the diffraction loss increases. When the difference in height is significant, the effect of one of the two obstacles is negligible compared to the other, the source of loss is considered as the most dominant obstacle.

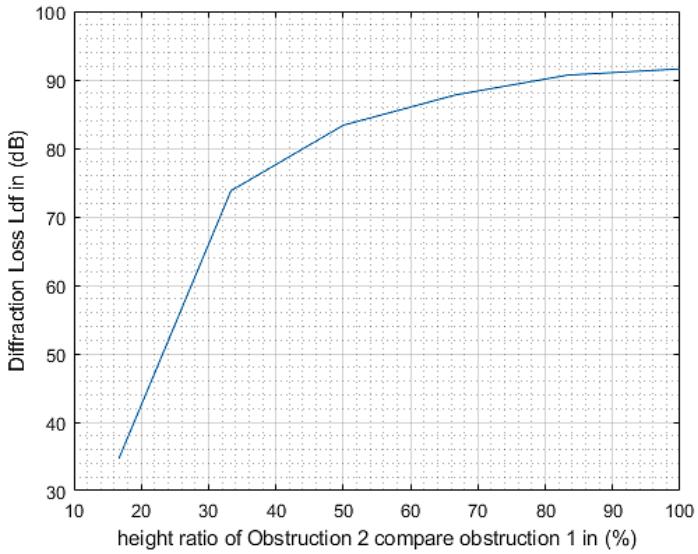

Figure 7. Effect of height ratio on diffraction loss using ITU-R model.

3.2.2. Effect of TX to Obstructing Object 1 Separation Distance a on Diffraction Loss

In this analysis, the effect of TX to obstructing object 1 separation distance on diffraction loss using ITU-R model at different frequencies (28 GHz, 38 GHz, 60 GHz, 73 GHz and 100 GHz) is considered where c, h_1, and h_2 are fixed at 40 m, 12 m, and 10 m. The TX to RX separation distance is supposed to be 200 m. The value of a is varied from 40 m to 140 m, and the value of b is given by:

$$b = d - (a + c) \text{ [m]} \tag{13}$$

A plot of diffraction loss in terms of a is illustrated in Fig. 8. As shown in Fig. 8, the effect of diffraction loss is correctly proportional to the frequency of the channel where when the distance a increases, the diffraction loss decreases.

3.2.3. Effect of Wavelength on Diffraction Loss

We study the wavelength effects on diffraction loss using ITU-R model, where the values of a, b, c, h_1, and h_2 are set to 40 m, 120 m, 40 m, 12 m, and 10 m, respectively. λ values correspond to the frequencies: 28 GHz, 38 GHz, 60 GHz, 73 GHz, and 100 GHz. This simulation is significant since the effect of the

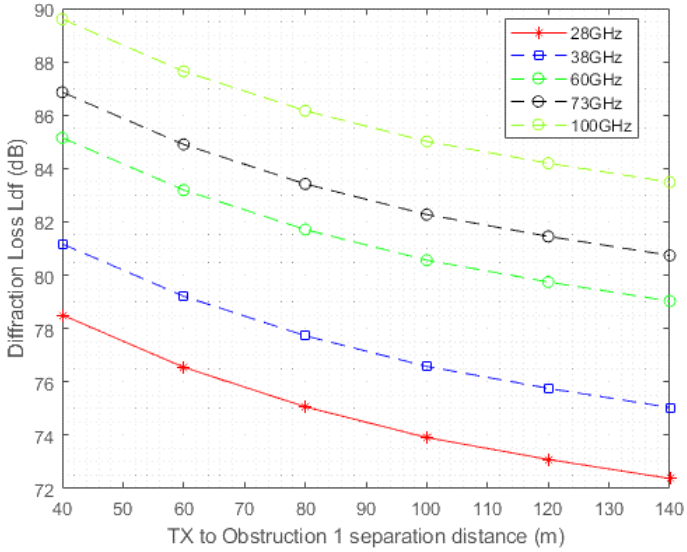

Figure 8. Effect of TX to obstructing object 1 separation distance on diffraction loss using ITU-R model.

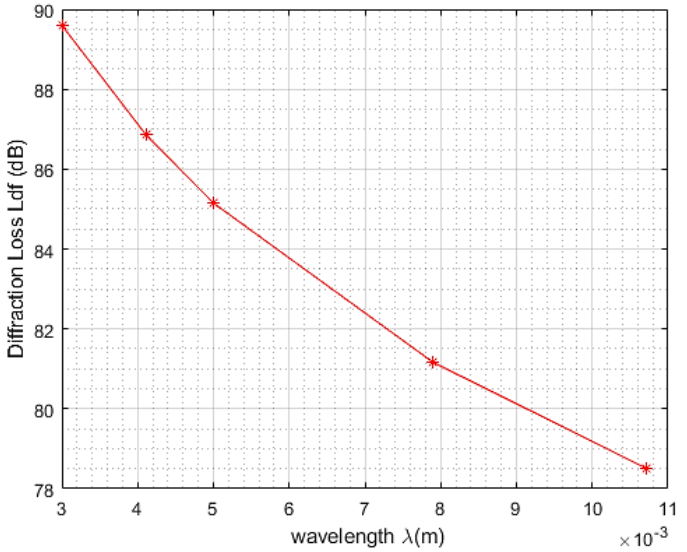

Figure 9. Effect of wavelength on diffraction loss using ITU-R model.

frequency band for point-to-point links depends on location and the environment of the country. Fig. 9 shows that the diffraction loss is inversely proportional with wavelength.

3.2.4. Effect of TX to RX Separation Distance on Diffraction Loss

In this analysis, we suppose that TX/RX connection employed at frequency 100 GHz with different values of TX/RX distance (d) is used. c, h_1, and h_2 values are fixed at 40 m, 12 m, and 10 m. In each value of d (200 m, 400 m, 600 m, and 800 m), the TX to obstructing object 1 separation distance a was assorted from 40 m to 140 m, 40 m to 340 m, 40 m to 540 m, and 40 m to 740 m, respectively. Fig. 10 shows the effect TX to RX separation distance on diffraction loss in ITU-R model.

As shown in Fig. 10, all the plots have the same curvature for inter-site distances, and to optimize the coverage zone of the multipath mmWave connection, the site where the diffraction loss is very

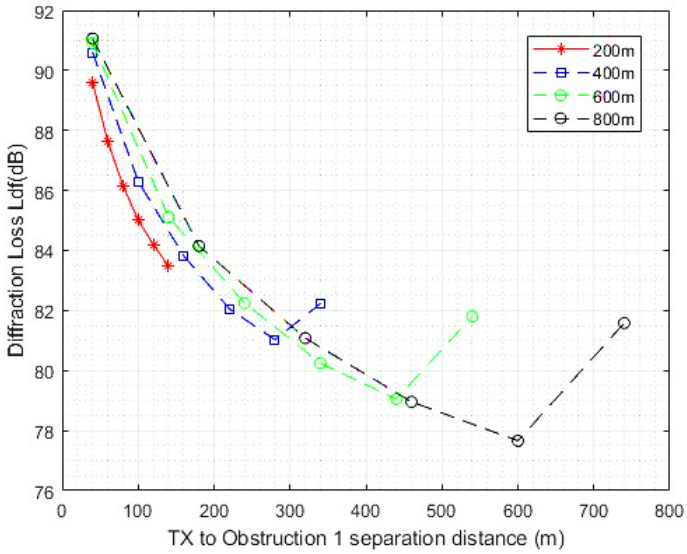

Figure 10. Effect of TX to RX separation distance on diffraction loss using ITU-R model.

significant denotes the locations after which the mmWave link cannot search for diffracting points. The area that extends from the transmitter to receiver for a distance of 800 m is considered as the most affected region by diffraction. This area is less affected as the length of the link increases.

3.3. Double Isolated Single Knife Edge Using Bullington Model

3.3.1. Effect of Height Ratio on Diffraction Loss

Figure 11 shows the effect of height ratio on diffraction using Bullington model. The values of a, b, c, and f were set at 40 m, 120 m, 40 m, and 100 GHz, respectively. Otherwise, h_1 is fixed at 12 m and h_2 varied from 2 m to 12 m. As the height ratio increases, the diffraction loss increases. When the difference in height is significant, the effect of one of the two obstacles is negligible compared to the other, the source of loss is considered as the most dominant obstacle.

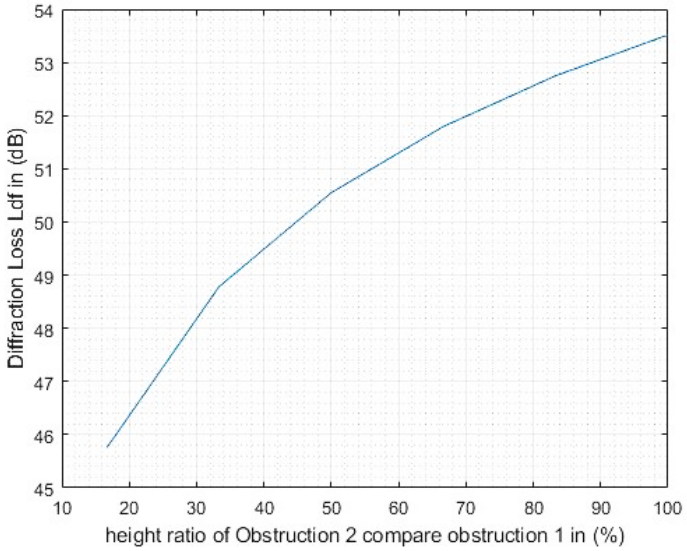

Figure 11. Effect of height ratio on diffraction loss using Bullington model.

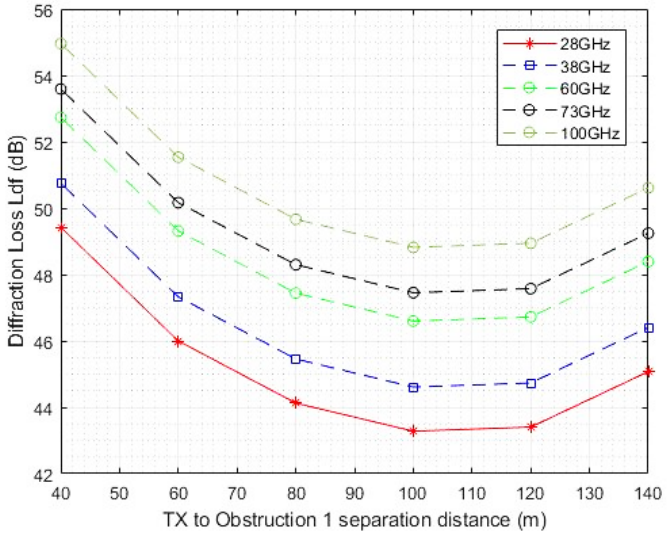

Figure 12. Effect TX to obstructing object 1 separation distance on diffraction loss using Bullington model.

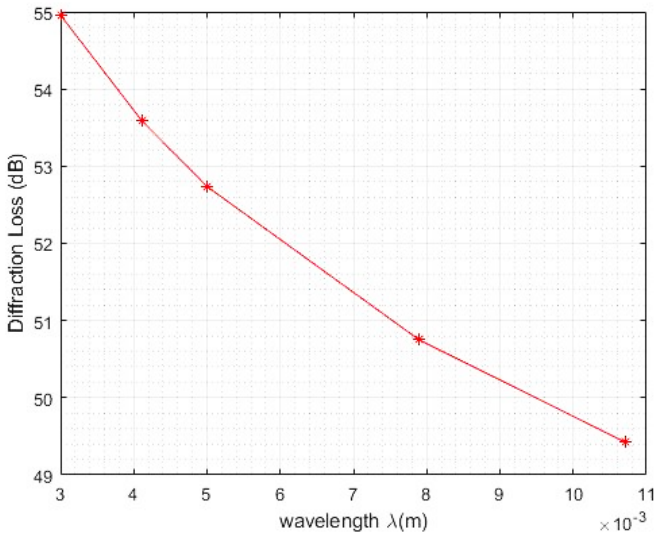

Figure 13. Effect of wavelength on diffraction loss using Bullington model.

3.3.2. Effect of TX to Obstructing Object 1a on Diffraction Loss

In this analysis, the effect of TX to obstructing object 1 separation distance on diffraction loss using Bullington model at different frequencies (28 GHz, 38 GHz, 60 GHz, 73 GHz, and 100 GHz) is considered where c, h_1, and h_2 are fixed at 40 m, 12 m, and 10 m. The TX to RX separation distance is supposed to be 200 m. The value of a is varied from 40 m to 140 m, and the value of b is given by: $b = d - (a + c)$ [m].

A plot of diffraction loss as a function of a is shown in Fig. 12. As show in Fig. 12, for all channels, we can see that the losses are larger as the obstructing abject 1 is near TX or RX antenna, and the effect of diffraction loss is correctly proportional to the frequency of the channel.

3.3.3. Effect of Wavelength on Diffraction Loss

In analyzing the effect of wavelength λ on the diffraction loss using Bullington model, where the values of a, b, c, h_1, and h_2 are set to 40 m, 120 m, 40 m, 12 m, and 10 m, respectively, where λ values correspond

to the frequencies: 28 GHz, 38 GHz, 60 GHz, 73 GHz, and 100 GHz. This simulation is significant since the effect of the frequency band for point-to-point links depends on location and the environment of the country. Fig. 13 shows that the diffraction loss is inversely proportional to wavelength.

3.3.4. Variation of Diffraction Loss with Transmitter to Receiver Distance

We suppose working at 100 GHz with a wavelength of 0.003 m where different values of TX/RX distance (d) are used. The values of c, h_1, and h_2 are fixed at 40 m, 12 m, and 10 m, respectively. At each value of d (200 m, 400 m, 600 m, and 800 m), the TX to obstructing object 1 separation distance a was varied from 40 m to 140 m, 40 m to 340 m, 40 m to 540 m, and 40 m to 740 m, respectively. Fig. 14 shows the effect of TX to RX separation distance on diffraction loss using Bullington model.

As shown in Fig. 14, all the plots have the same curvature for inter-site distances, and to optimize the coverage zone of the multipath mmWave connection, the site where the diffraction loss is very significant denotes the locations after which the mmWave link cannot search for diffracting points. The area that extends from the transmitter to receiver for a distance of 800 meters is considered as the most affected region by diffraction. This area is less affected as the length of the link increases.

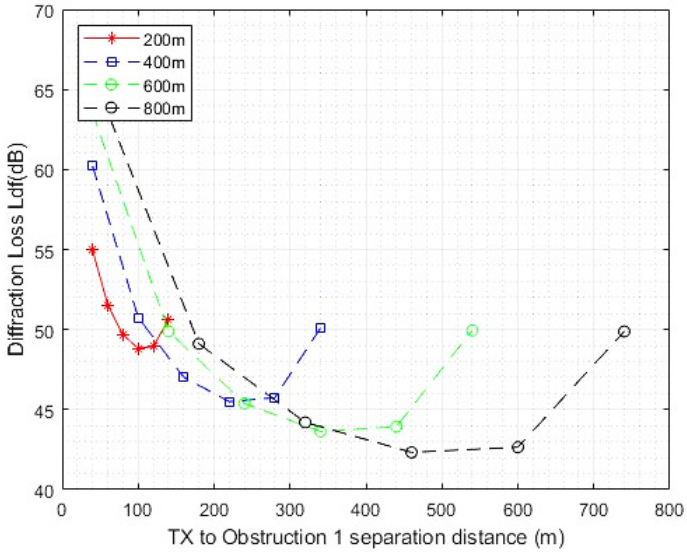

Figure 14. Effect of TX to RX separation distance on diffraction loss using Bullington model.

4. CONCLUSION

This paper presents the results of diffraction loss over the rooftop of building at 28 GHz, 38 GHz, 60 GHz, 73 GHz, and 100 GHz in terms of large ranges of diffraction angles and distances in an urban microcell area. One model of diffraction called the Knife Edge diffraction (KED) including two main models, Single Knife Edge diffraction (SKED) and Double Isolated Single (DISKED) model, adopted to study the mentioned mmWaves bands. We focused on ITU Recommendation (ITU-R P.526-15, 10/2019). Based on the results of our studies, it has been shown that the diffraction losses are inversely proportional to the distance between obscuring object and transmitter, wavelength and the distance between TX and RX. The effects on the diffraction loss as shown in DISKED results are very significant compared to that in the SKED results. This helps to determine typical diffraction loss values and corresponding parametric values to be used for above-rooftop propagation in urban environments in the case of millimeter wave. The analysis on mmWave bands would be useful to explore and develop the measurable channel model for 5G/6G millimeter wave communications. Otherwise, this information is valuable input in the design of an NLOS small cell backhaul system. Hopefully, it can be utilized as a reference for the evolution of future wireless systems.

As a perspective, it is recommended to study the terahertz bands which can provide large band requests for 5G and 6G wireless technology. Terahertz frequency located on a spectrum ranging between 0.1 THz and 10 THz waves which is a candidate to be used in the development of 6G, where "terahertz waves" have the problem that the radio wave rectilinear property is greater than that of the millimeter wave and does not propagate far.

ACKNOWLEDGMENT

This work is supported by Directorate General for Scientific Research and Technological Development (DGRSDT), Ministry of Higher Education and Scientific Research — Algeria.

REFERENCES

1. FCC Press Release, Mar. 2019. Available: https://docs.fcc.gov/public/attachments/DOC-356588A1.pdf.
2. Marcus, M. J., "Progress in opening access to spectrum above 100 GHz," *IEEE Wireless Communications*, Vol. 26, No. 2, 2–3, 2019.
3. Rec. ITU-R P.1411–8, "Propagation data and prediction methods for the planning of short-range outdoor radiocommunication systems and radio local area networks in the frequency range 300 MHz to 100 GHz," *ITU-R Recommendation*, Vol. 8, P Series, ITU, Geneva, July 2015.
4. Zhan, Q., Y. Fang, M. Zhuang, et al., "Stabilized DG-PSTD method with non conformal meshes for electromagnetic waves," *IEEE Transactions on Antennas and Propagation*, Vol. 68, No. 6, 4714–4726, 2020.
5. Zhan, Q., Y. Wang, Y. Fang, et al., "An adaptive high-order transient algorithm to solve large-scale anisotropic Maxwell's equations," *IEEE Transactions on Antennas and Propagation*, Vol. 70, No. 3, 2082–2092, 2021.
6. Viriyasitavat, W., M. Boban, H.-M. Tsai, et al., "Vehicular communications: Survey and challenges of channel and propagation models," *IEEE Vehicular Technology Magazine*, Vol. 10, No. 2, 55–66, 2015.
7. Zekri, A. B., R. Ajgou, and M. Hettiri, "Impact of azimuth and elevation half power beam width on human blockage scenarios in mmWave channels," *Proceedings of the IEEE 1st International Conference on Communications, Control Systems and Signal Processing (CCSSP)*, 41–45, IEEE, El Oued, Algeria, May 2020.
8. Ahamed, M. M. and S. Faruque, "Propagation factors affecting the performance of 5G millimeter wave radio channel," *Proceeding of the IEEE International Conference on Electro Information Technology (EIT)*, 728–733, Grand Forks, ND, USA, May 2016.
9. Abdulrasool, A. S., J. S. Aziz, and S. J. Abou-Loukh, "Calculation algorithm for diffraction losses of multiple obstacles based on Epstein-Peterson approach," *International Journal of Antennas and Propagation*, Vol. 2017, Article ID 3932487, 9 pages, 2017, https://doi.org/10.1155/2017/3932487.
10. Walfisch, J. and H. L. Bertoni, "A theoretical model of UHF propagation in urban environments," *IEEE Transactions on Antennas and Propagation*, Vol. 36, No. 12, 1788–1796, 1988.
11. Hur, S., S. Baek, B. Kim, et al., "Proposal on millimeter-wave channel modeling for 5G cellular system," *IEEE Journal of Selected Topics in Signal Processing*, Vol. 10, No. 3, 454–469, 2016.
12. Lu, J. S., H. L. Bertoni, K. A. Remley, et al., "Site-specific models of the received power for radio communication in urban street canyons," *IEEE Transactions on Antennas and Propagation*, Vol. 62, No. 4, 2192–2200, 2014.
13. Mcnamara, D. A. and C. Pistotius, *Introduction to the Uniform Geometrical Theory of Diffraction*, 488, Artech House Microwave Library, 1990.
14. Keller, J., "Diffraction of a convex cylinder," *IRE Transactions on Antennas and Propagation*, Vol. 4, No. 3, 312–321, 1956.
15. Kouyoumjian, R. G. and P. H. Pathak, "A uniform geometrical theory of diffraction for an edge in a perfectly conducting surface," *Proceedings of the IEEE*, Vol. 62, No. 11, 1448–1461, 1974.

16. Pathak, P., W. Burnside, and R. Marhefka, "A uniform GTD analysis of the diffraction of electromagnetic waves by a smooth convex surface," *IEEE Transactions on Antennas and Propagation*, Vol. 28, No. 5, 631–642, 1980.
17. Luebbers, R., "Finite conductivity uniform GTD versus knife edge diffraction in prediction of propagation path loss," *IEEE Transactions on Antennas and Propagation*, Vol. 32, No. 1, 70–76, 1984.
18. Kim, K.-W., et al., "Diffraction loss model based on 28 GHz over-rooftop propagation measurements," *Proceeding of the IEEE 86th Vehicular Technology Conference (VTC-Fall)*, Toronto, ON, Canada, September 2017.
19. Kim, K.-W., M.-D. Kim, J. Lee, et al., "Millimeter-wave diffraction-loss model based on over-rooftop propagation measurements," *ETRI Journal*, Vol. 42, No. 6, 827–836, 2020.
20. Tervo, N., et al., "Diffraction measurements around a building corner at 10 GHz," *Proceeding of the IEEE 1st International Conference on 5G for Ubiquitous Connectivity*, Akaslompolo, Finland, November 2014.
21. Rappaport, T. S., G. R. Maccartney, S. Sun, et al., "Small-scale, local area, and transitional millimeter wave propagation for 5G communications," *IEEE Transactions on Antennas and Propagation*, Vol. 65, No. 12, 6474–6490, 2017.
22. Lu, J. S., et al., "Measurement and characterization of various outdoor 60 GHz diffracted and scattered paths," *Proceeding of the IEEE MILCOM 2013 — 2013 Military Communications Conference*, Diego, CA, USA, November 2013.
23. Anderson, H. R., "Building corner diffraction measurements and predictions using UTD," *IEEE Transactions on Antennas and Propagation*, Vol. 46, No. 2, 292–293, 1998.
24. Recommendation ITU-R P.526-15, "Propagation by diffraction," 2019.
25. Viswanathan, M., *Wireless Communications Systems in MATLAB*, 2nd Edition, June 8, 2020.
26. Jacob, M., S. Priebe, A. Maltsev, et al., "A ray tracing based stochastic human blockage model for the IEEE 802.11 ad 60 GHz channel model," *Proceedings of the IEEE 5th European Conference on Antennas and Propagation (EUCAP)*, 3084–3088, Rome, Italy, April 2011.
27. Kunisch, J. and J. Pamp, "Ultra-wideband double vertical knife-edge model for obstruction of a ray by a person," *Proceeding of the IEEE International Conference on Ultra-Wideband*, 17–20, Hannover, Germany, September 2008.
28. Jacob, M., S. Priebe, R. Dickhoff, et al., "Diffraction in mm and sub-mm wave indoor propagation channels," *IEEE Transactions on Microwave Theory and Techniques*, Vol. 60, No. 3, 833–844, 2012.
29. Ghasemi, A., A. Abedi, and F. Ghasemi, *Propagation Engineering in Wireless Communications*, Springer, New York, NY, USA, 2016.
30. Takada, J.-I., K. Murakami, P. Hanpinitsak, et al., "Experimental evaluation of over-the-rooftop propagation loss prediction model for the spectrum sharing at 26 GHz band," *International Applied Computational Electromagnetics Society Symposium (ACES)*, 1–3, IEEE, Hamilton, ON, Canada, August 2021.
31. Ellis, T. and S. Weiss, "Propagation prediction for rail communications in urbanized areas," *Proceedings of the 2018 Joint Rail Conference, 2018 Joint Rail Conference*, Pittsburgh, Pennsylvania, USA, April 18–20, 2018, V001T03A006, ASME, https://doi.org/10.1115/JRC2018-6196.
32. Asen, W., "Comparison of measurements with prediction methods for propagation by diffraction at 88–108 MHz," *IEEE Transactions on Antennas and Propagation*, Vol. 52, No. 6, 1499–1504, 2004.
33. Sheikh, A. U. H., *Wireless Communications: Theory and Techniques*, Springer Science & Business Media, 2004.
34. Sasaki, M., M. Inomata, W. Yamada, et al., "Path loss model considering blockage effects of traffic signs up to 40 GHz in urban microcell environments," *IEICE Transactions on Communications*, Vol. 101, No. 8, 1891–1902, 2018.